



Euonymus laxiflorus Champ. Bioactive Compounds Inhibited α -Glucosidase and Protein Phosphatase 1B – A Computational Approach Towards the Discovery of Antidiabetic Drugs

Phan T. Quy¹, Thanh Q. Bui², Nguyen V. Bon³, Phan T. K. Phung^{4,5}, Duong P.N. Duc⁶, Dang T. Nhan⁷,
Nguyen V. Phu⁸, Dao C. To⁹, Nguyen T. A. Nhung^{2*}

¹Department of Natural Sciences & Technology, Tay Nguyen University, Buon Ma Thuot 630000, Vietnam

²Department of Chemistry, University of Sciences, Hue University, Hue 530000, Vietnam

³Institute of Biotechnology and Environment, Tay Nguyen University, Buon Ma Thuot 630000, Vietnam

⁴Faculty of Medicine and Pharmacy, Tay Nguyen University, Buon Ma Thuot 630000, Vietnam

⁵Faculty of Pharmacy, University of Medicine and Pharmacy at Ho Chi Minh City, Ho Chi Minh City 700000, Vietnam

⁶Faculty of Traditional Medicine, University of Medicine and Pharmacy at Ho Chi Minh City, Ho Chi Minh City 700000, Vietnam

⁷Faculty of Forestry Agriculture, Tay Nguyen University, Buon Ma Thuot 630000, Vietnam

⁸Faculty of Basic Sciences, University of Medicine and Pharmacy, Hue University, Hue 530000, Vietnam

⁹Phenikaa University Nano Institute (PHENA), Phenikaa University, Yen Nghia, Ha Dong district, Hanoi 12116, Vietnam

ARTICLE INFO

Article history:

Received 10 April 2023

Revised 26 May 2023

Accepted 26 May 2023

Published online 01 June 2023

Copyright: © 2023 Quy *et al.* This is an open-access article distributed under the terms of the [Creative Commons Attribution License](https://creativecommons.org/licenses/by/4.0/), which permits unrestricted use, distribution, and reproduction in any medium, provided the original author and source are credited.

ABSTRACT

Euonymus laxiflorus Champ. has recently proven for its antidiabetic potential yet its ingredient-activity relationship is vastly unknown. A combination of quantum calculation, molecular docking simulation, physicochemical analysis, and ADMET was utilised together for the theoretical argument on potentiality of bioactively undetermined components (1-15) against α -glucosidase (PDB-3W37) and tyrosine phosphatase 1B (UniProtKB-PTP1B). Dipole moment values indicate the favoured bio-medium compatibility of 10 (6.370 Debye), 12 (6.381 Debye), and 15 (8.446 Debye), while the values discourage the potential of 5 (0.792 Debye) and 11 (0.905 Debye). Molecular electrostatic potential maps imply the intermolecular interacting flexibility of 6-10 and 12-15. Docking-based simulation predicts the most effective inhibitory systems, i.e. (i) ligand-3W37: 10 \approx 11 (DS -11.7 kcal.mol⁻¹) \approx 3 (DS -11.6 kcal.mol⁻¹) > 7 \approx 12 (DS -11.1 kcal.mol⁻¹); (ii) ligand-PTP1B: 11 (DS -12.0 kcal.mol⁻¹) > 13 (DS -11.8 kcal.mol⁻¹) > 5 (DS -11.2 kcal.mol⁻¹) > 3 (DS -11.0 kcal.mol⁻¹). Polarisability justifies the bio-medium compatibility of 10 (70.8 Å³) and 15 (64.7 Å³) while especially opposes the potentiality of 11 (19.1 Å³). Physicochemical and pharmacological properties support the suitability for further drug-like development. Altogether, 10 (7-Hydroxy-6,7-dihydro-cis/trans-geraniate, 3-O- α -L-arabinopyranosyl (1 \rightarrow 6)- β -D-glucopyranosyl) and 15 (3,5-dimethoxy-4-hydroxyphenol)-1-O- β -D-(6'-O-galloyl)-glucopyranoside) are allocated as the most promising antidiabetic inhibitors.

Keywords: Celastraceae; *Euonymus laxiflorus*; quantum chemical calculation; molecular docking simulation; QSARIS; ADMET

Introduction

Diabetes mellitus has been rising as a worldwide concern on health, quality of life, and life expectancy, thus putting pressure on healthcare systems. The disease is known as a chronic glucose-related metabolic disorder often resulting in hyperglycemia, which in-turn induces to further complications reported by diverse epidemiological studies and clinical trials.¹⁻⁵ The causes are of low certainty, possibly due to genetic abnormalities, pathologic disorders, clinical conditions, or gestational failures.⁶

*Corresponding author. E mail: ntanhung@hueuni.edu.vn
Tel: +84986980263

Citation: Quy PT, Bui TQ, Bon NV, Phung PTK, Duc DPN, Nhan DT, Phu NV, To DC, Nhung NTA. *Euonymus laxiflorus* Champ. Bioactive Compounds Inhibited α -Glucosidase and Protein Phosphatase 1B – A Computational Approach Towards the Discovery of Antidiabetic Drugs. Trop J Nat Prod Res. 2023; 7(5):2946-2964. <http://www.doi.org/10.26538/tjnpr/v7i5.21>

Official Journal of Natural Product Research Group, Faculty of Pharmacy, University of Benin, Benin City, Nigeria.

The prevalence of diabetic conditions is well recorded by two main biological mechanisms: i.e. the destruction of pancreatic β -cells (type 1) and the abnormal activity of insulin metabolism (type 2); particularly, the latter accounts for 90-95 % of cases.⁷ This justifies the inhibition of glucose- and insulin-based enzymes as the main strategy for diabetic therapeutic treatments and symptomatic remedies. In essence, α -glucosidase-based inhibitors act against the hydrolysis of (1/4) and (1/6) bonds in starch and disaccharide molecules, which are extensively expressed in food sources such as microbes, plants, and animal tissues, thus reducing postprandial spikes from digestive carbohydrates.^{8,9} Meanwhile, potential inhibitors against protein tyrosine phosphatase 1B activity would cut off the phosphorylation, which is responsible for activation of the insulin responsive cell (receptor) for glucose uptake; in other words, PTP1B-based inhibitors provide a negative regulatory effect to the insulin signalling pathway, inducing a reduction of glucose uptake.¹⁰ Given the well-established knowledge, α -glucosidase and tyrosine phosphatase 1B can be considered as anti-diabetic targeted enzymes for regulation of blood glucose level. In the existing literature, the biological assemblies of the proteins have been well-determined using different experimental methods and deposited onto public online protein banks, e.g. 3W37 (DOI: 10.2210/pdb3W37/pdb) for α -glucosidase and PTP1B (DOI: UniProtKB-A0A0U1XP67) for tyrosine phosphatase 1B. On commercial market, a variety of hypoglycemic drugs have been prescribed for treatment of diabetes, e.g. sulfonylureas,

biguanides, or acarbose; however, the substances are also known with mild-serious side effects, e.g. diarrhea or flatulence.^{11,12} Furthermore, intravenous injection of insulin on the daily basis is required. Therefore, new, effective, and safe antidiabetic agents are still the subjects of research interest, especially those from digestible natural sources (herbs and medicinal plants); for example, even a household flavouring herb such as garlic was recently found to possess untouched anti-diabetic potential against α -amylase and α -glucosidase.¹³

Euonymus laxiflorus Champ. (the Celastraceae family) is a subtropical shrub (biome), native to South India, South China, Taiwan and the Indochinese peninsula. According to folk experiences, the plant is known as a valuable medicinal plant possessing a variety of biological activities, e.g. remediation of osteoarthritis, inflammatory arthritis, and haemostasis. It particularly has long used as a traditional medicine by the ethnic people in Dak Lak, Vietnam. According to recent findings, the anti-oxidant,¹⁴ anti-inflammatory,¹⁵ anti-cancerous,¹⁶ and anti-diabetic¹⁷ activities have been preliminarily tested and experimentally evidenced. In 2003, Kou *et al.* first-time reported 11 components extracted and isolated from Taiwan-based *E. laxiflorus* arial parts. In 2017, our Institute of Cancer Research (ICR) mouse model revealed the hypoglycemic effect of the total methanol extract of *E. laxiflorus* Champ. trunk bark¹⁴ and its major component (condensed tannin)¹⁸ given by the reduction of plasma glucose levels in diabetic laboratory mice. In 2018, our group reported 25 compounds identified in the methanol extracts of the bark, which afterwards were subjected for a variety of biological activities including antidiabetics against α -glucosidase and α -amylase¹⁹. The findings are summarised in Table 1. However, the trials were incomplete as the bioassays were only carried out on only certain candidates with sufficient degree of quantity extracted and quality purified. Therefore, more efforts are still needed to evaluate the potential of the biologically undetermined candidates, thus justifying further attempts for either cumulative isolation or pre-clinical tests; nevertheless, their high bio-versatility yet low content might put considerable challenges from the view of experimental trials. From the standpoint of *in silico* prescreening research, the promising candidates can be quickly allocated based on desirable properties. By

the aid of computer-based power, the cost and time for equivalent wet lab-works can be significantly reduced. If utilised with appropriate flexibility, the results from certain different theoretical platforms can converge to predictions with high degree of accuracy and reliability. In particular, *ab initio* calculation can provide information on the electronic properties, hence possibly chemical potential maps of a structure; in consequence, its intermolecular interactability can be deduced. On the other hand, molecular docking simulation can render the ligand-protein interacting configurations for prediction on the conformation of candidate inhibitors and their targeted binding sites,²⁰ which is significantly useful in structure-based drug design. However, most algorithms apply the concept of static pseudo-Gibbs free energy²¹ and ignore the pre-docking conditions, such as physio-chemical resistance. This weakness can be reconciled finely with the incorporation of the physicochemical properties of the candidates. In fact, we proved this approach based on the experiment-theory correlations observed from the antidiabetic activities of *Dolichandrone spathacea* catalpol²² and *Dipterocarpus alatus* dipterocarpol²³ derivatives. Also, there are statistically regressive models for prediction of pharmacokinetics and pharmacological properties if a chemical structure is available as the input, e.g. SwissADME. Altogether, these computational implementations can provide reliable and consistent view on the bio-compatible and pharma-suitable potentiality of a large number of compounds. As an example, Adelusi *et al.* recently harness the advantages of molecular dynamics, quantum mechanics, and docking technique to explore the inhibitory potentials of various natural products²⁴⁻²⁶.

In this extension, candidates with undetermined diabetic activity were selected for computer-based combinatory research, including density functional theory (DFT) calculation, molecular docking simulation, and statistical regressions of physicochemical (using QSARIS) and pharmacological (using SwissADME) properties. The output serves as the prediction for inhibitory effectiveness of the candidates against two types of diabetes-related enzymes, i.e. α -glucosidase and tyrosine phosphatase 1B, collecting knowledge to the existing literature and justifying further experimental attempts.

Table 1: Summary of *Euonymus laxiflorus* components isolated and their determined bioactivities

No	Compound	Bioactivities (IC ₅₀ $\mu\text{g.mL}^{-1}$)		
		α -glucosidase inhibition ¹⁸	α -amylase inhibition ¹⁹	Oxidation inhibition ¹⁵
	Vietnam-based <i>Euonymus laxiflorus</i> Champ.			
1	Walterolactone A/B β -D-pyranoglucoside,	0.907	123	28
2	1- β -D-Glucopyranosyloxy-3,5-dimethoxy-4-hydroxybenzene	UD	UD	58.11
3	(-)-Gallocatechin	11.9	121	30.73
4	Schweinfurthinol 9-O- β -D-pyranoglucoside	31.6	≥ 290	UD
5	1-O-(3-Methyl)-butenoyl-myo-inositol	27.1	≥ 1094	UD
6	Leonuride	0.926	39.6	27.47
7	(+)-Catechin	0.113	7.1	7.10
8	Methyl galloate	110	≥ 330	9.4
9	(-)-Catechin	UD	≥ 370	UD
10	Gallic acid	UD	281	9
11	Condensed tannin	0.076	0.74	UD
12	(3,5-dimethoxy-4-hydroxyphenol)-1-O- β -D-(6'-O-galloyl)-glucopyranoside	UD	≥ 128	7.8
13	Umbelactone	UD	UD	NA
14	Walterolactone	UD	UD	NA
15	Phenylalanine	UD	UD	NA
16	2-methoxy-4-hydroxyphenol-1-O- β -D-glucopyranoside	UD	UD	38.09
17	3,4-Dihydroxybenzoic acid	UD	UD	16.77
18	2-benzoyl myo-inositol	UD	UD	NA
19	1-O-Benzoyl-myo-inositol	UD	UD	NA

20	Walterolactone A/B 6- <i>O</i> -gallate- β -D-glucopyranoside	UD	UD	10.9
21	Roseoside (6S, 9S)	UD	UD	NA
22	(3R*,6R*)-tetrahydro-6-ethenyl-2,2,6-trimethyl-2H-pyran 3- <i>O</i> - α -L-arabinopyranosyl (1 \rightarrow 3)- β -D-glucuronopyranosyl	UD	UD	UD
23	7-Hydroxy-6,7-dihydro-cis/trans-geraniate, 3- <i>O</i> - α -L-arabinopyranosyl (1 \rightarrow 6)- β -D-glucopyranosyl	UD	UD	UD
24	1-(4-hydroxyphenyl)-2,3-dihydroxypropan-1-one 3- <i>O</i> - β -D-glucopyranoside/or Schweinfurthinol 9- <i>O</i> - β -D-glucopyranoside	UD	UD	NA
25	Myo-inositol 1- <i>O</i> -3,3-dimethylacrylate/or 1- <i>O</i> -(3-methyl)-butenoyl-myo-inositol	UD	UD	NA
Taiwan-based <i>Euonymus laxiflorus</i>		Anti-inflammatory activity ¹⁶		Anticarcinogenic activity ¹⁶
26	Laxifolone A	0.12	≥ 20	4 cell lines
27	Ebenifoline E-II	UD	≥ 20	4 cell lines
28	Euojaponine C	UD	≥ 20	4 cell lines
29	Emarginatine E	UD	1.7	KB
			4.1	COLO-205
30	12-en-22,29-gamma-lactone	UD	≥ 20	4 cell lines
31	3,11-dioxo-beta-amyrene	UD	≥ 20	4 cell lines
32	3beta, 22alpha-dihydroxyolean-12-en-29-oic acid	UD	≥ 20	4 cell lines
33	28,29-dihydroxyfriedelan-3-one	UD	≥ 20	4 cell lines
34	29-hydroxy -3-oxo-D	UD	≥ 20	4 cell lines
35	A-Friedooleanan-28-oic acid	UD	≥ 20	4 cell lines
36	Putranjivadione	UD	≥ 20	4 cell lines

UD: undetermined; NA: no activity;

4 cell lines: nasopharynx carcinoma (KB), colon carcinoma (COLO-205), hepatoma (Hepa-3B), and cervical carcinoma (Hela) cells

Methodology

Table 2 includes the selected ligands and their notations (1-15) used as the input for computational modelling in this work.

Quantum chemical calculation

Molecular quantum properties were obtained from density functional theory (DFT) calculation on Gaussian 09; no symmetry constraints;²⁷ level of theory B3LYP/6-311++G(d,p);²⁸ basis set def2-TZVPP.²⁹ The global minimum on potential energy surface (PES) was confirmed by vibrational frequencies. The frozen-core approximation for non-valence-shell electrons and the resolution-of-identity (RI) approximation were applied. The configurations were used to calculation of optimised geometries, potential energy surface (PES), dipole moments, and molecular electrostatic potential (MEP).

Molecular docking simulation

Ligand-protein static inhibibility can be evaluated using MOE 2015.10³⁰ based on the molecular docking technique. In a typical procedure, the simulation follows four steps and results in ligand-protein complex structures, accordingly. Input preparation: Protein assemblies of α -glucosidase (3W37; PDB DOI: 10.2210/pdb3W37/pdb) and tyrosine phosphatase 1B (PTP1B; ID: UniProtKB-A0A0U1XP67) were referenced from public online protein banks; active-gird range: 4.5 Å from amino acids; force field: MMFF94x; Tether-Receptor strength: 5000; energy resolution: 0.0001 kcal.mol⁻¹.Å⁻¹. Ligand structures were from those selected from our previous works; geometrical optimisation: Conj Grad algorithm; energy-change termination: 0.0001 kcal.mol⁻¹; charge assignment: Gasteiger-Huckel method; Docking simulation: Ligand-protein interaction was simulated; number of retaining poses = 10; maximum solutions per iteration = 1000; maximum solutions per fragmentation = 200; Re-docking iteration: The inhibitory components

(ligand and protein) were separated, then re-docked. The accuracy of the docking protocol is justified if RMSD values (of docked and re-docked conformations) are all under 2 Å; Theoretical interpretation: The primary parameters for inhibitory effectiveness are docking score (DS) energy, root-mean-square deviation (RMSD) value, and numbers of hydrophilic binding (hydrogen-like bonds). Besides, ligand-protein interactions and in-pose arrangement were mapped and rendered on 2D and 3D visualization, respectively.

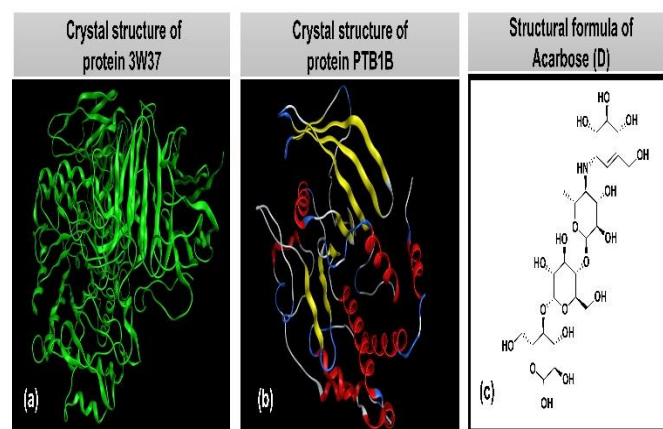


Figure 1: Crystal structures of (A) α -glucosidase protein (PDB-3W37; DOI: 10.2210/pdb3W37/pdb); (B) tyrosine phosphatase 1B (PTP1B; ID: UniProtKB-A0A0U1XP67); and (C) structural formula of controlled drug Acarbose (D)

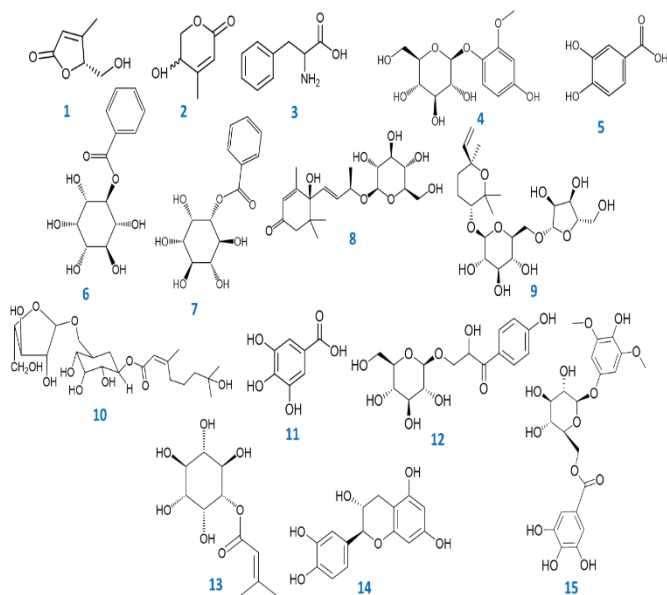


Figure 2: Investigated compounds (1-15) isolated from *Euonymus laxiflorus* Champ

Figure 1 shows the crystal structures of α -glucosidase, protein tyrosine phosphatase 1B, and the controlled drug Acarbose. Figure 2 presents the chemical formulas of selected ligands as the input for docking simulation. The protein assemblies were determined experimentally by other works and the potential inhibitors were from our preceding report.

QSARIS-based analysis

Drug-likeness properties of the phytochemicals were predicted by a combinational model, including (i) Parameters: QSARIS-derived physical properties (based on Gasteiger–Marsili method³¹); (ii) Reference: Lipinski's rule of five.³² The former includes molecular mass (Da), polarisability (\AA^3), size (\AA), and dispersion coefficients ($\log P$ and $\log S$); on the other side, the rule sets criteria for a well membrane-permeable candidate, i.e (i) Molecular mass < 500 Da; (ii) hydrogen-bond donors ≤ 5 ; (iii) hydrogen-bond acceptors ≤ 10 ; (iv) $\log P < +5$.^{33,34}

ADMET-based analysis

ADMET properties (absorption, distribution, metabolism, excretion, and toxicity) were obtained from a web-based regressive model developed and maintained by the Molecular Modeling Group, Swiss Institute of Bioinformatics, i.e. SwissADME (<http://www.swissadme.ch/>; April 2nd, 2023). The theoretical interpretations of output pharmacokinetic parameters were described by Pires *et al.*³⁵ and powered by the University of Melbourne and University of Cambridge for public reference (<http://biosig.unimelb.edu.au/pkcsdm/theory>; April 2nd, 2023).

Table 2: Bioactive compounds (1-15) used as computational input in this study

Notation	Nomenclature	Formula
1	Umbelactone	C ₆ H ₈ O ₃
2	Walterolactone	C ₆ H ₈ O ₃
3	Phenylalanine	C ₉ H ₁₁ NO ₂
4	Isotachioside	C ₁₃ H ₁₈ O ₈
5	3,4-Dihydroxybenzoic acid	C ₇ H ₆ O ₄
6	(1S,2R,3S,4S,5S,6S)-2,3,4,5,6-pentahydroxycyclohexyl benzoate	C ₁₃ H ₁₆ O ₇
7	(1R,2S,3R,4S,5S,6S)-2,3,4,5,6-pentahydroxycyclohexyl benzoate	C ₁₃ H ₁₆ O ₇
8	Roseoside	C ₁₉ H ₃₀ O ₈
9	(2S,3R,4R,5S,6R)-2-(((2S,3S,4R,5S)-3,4-dihydroxy-5-(hydroxymethyl)tetrahydrofuran-2-yl)oxy)methyl)-6-(((3R,6S)-2,2,6-trimethyl-6-vinyltetrahydro-2H-pyran-3-yl)oxy)tetrahydro-2H-pyran-3,4,5-triol	C ₂₁ H ₃₆ O ₁₁
10	7-Hydroxy-6,7-dihydro-cis/trans-geraniate, 3-O- α -L-arabinopyranosyl (1 \rightarrow 6)- β -D-glucopyranosyl	C ₂₂ H ₃₈ O ₁₁
11	Gallic acid	C ₇ H ₆ O ₅
12	1-(4-hydroxyphenyl)-2,3-dihydroxypropan-1-one 3-O- β -D-glucopyranoside	C ₁₅ H ₂₀ O ₉
13	Myo-inositol 1-O-3,3-dimethylacrylate	C ₁₁ H ₁₈ O ₇
14	(-)-Catechin	C ₁₅ H ₁₄ O ₆
15	3,5-dimethoxy-4-hydroxyphenol-1-O- β -D-(6'-O-galloyl)-glucopyranoside	C ₂₁ H ₂₄ O ₁₃

Results And Discussion

In this report, the results retrieved from different computational platforms serve different purposes on the theoretical argument, and altogether predict the promising candidates for antidiabetic potential. In particular, ground state energy and dipole moment (given by quantum calculation) provide the views on bio-chemical stability and bio-medium compatibility, respectively; docking-score values (given by molecular docking simulation) are ranked into the order of static inhibitory effectiveness; QSARIS-based physicochemical properties coupled with Lipinski's criteria evaluate the drug likeness and polarized interactability; ADMET-based pharmacological properties in reference to Pires' interpretations justify the potentiality of medicinal development.

DFT-based chemical properties

The results from quantum calculation include the optimised structural geometries and electronic configurations, used to argue their certain *ab initio* insights of chemical potentials in intermolecular interactability. This is based on the intrinsic chemical properties of each bioactive compounds (1-15) away from any targeted proteins.

Figure 3 presents the converged geometries and Table 3 summarised their corresponding molecular properties (i.e. ground state energy and dipole moment). Overall, the convergence can be reached without any geometrical constraints or abnormal bonding parameters (i.e. angles and length). This implies their stability often seen in natural compounds, thus in-turn confirming our preceding spectroscopic characterisation and structural elucidation. For instance, the length figures vary marginally within the characteristic ranges for C–C (ca. 1.5 \AA), C=C (ca. 1.3 \AA), C–H (ca. 1.1 \AA), C–O (ca. 1.4 \AA), C=O (ca. 1.2 \AA), N–C (ca.

1.4 Å); while, the aromatic ring are in-planar. Their negative ground-state energy (all under -400 a.u.) also means that they are less likely to be sensitive to chemical reacting attacks, thus more likely to be conducive to bio-inhibitory applications. Noticeably, 10 and 15 (ca. -1700 a.u.) register the most pronounced values; they are followed by 9 (ca. -1650 a.u.). These are the candidates with least likely to have serious physiochemical effects, thus most likely inert in bio-chemical media and suitable for inhibitory applications. On the other hand, 1 and 2 (ca. -450 a.u.) might be considered as least promising. However, it is noteworthy that these argument does not ensure the complete chemical inertia nor serious harms of the compounds given by their activity in the body; in fact, this only argues the relative tendency. Regarding dipole moment, 1 (5.039 Debye), 2 (5.241 Debye), 4 (4.240 Debye), 10 (6.370 Debye), 12 (6.381 Debye), and 15 (8.446 Debye) register predominant values, especially the last three. In principle, dipole moment is the positive-negative charge separation in a system, thus measuring the compatibility with a dipole-solvent environment, such as physiochemical media. Therefore, 10, 12, and 15 might be considered particularly suitable for biological applications in general and protein-inhibited interactions (based on van der Waals forces or ionic bonds³⁶) in particular. In contrast, 5 (0.792 Debye) and 11 (0.905 Debye) should be not highly recommended for these practices from this theoretical argument.

Figure 4 provides molecular electronic potential (MEP) maps of the optimised structures, the distribution of chemical activities over their molecular plane. By convention, reddish colours represent the negative electrostatic potential (i.e. rich in electron density); this means that the regions might serve as a nucleophilic site in chemical reactions yet an electron donor in intermolecular interactions. In contrast, bluish colours represent positive electrostatic potential (i.e. related to electrophilic reactivity). Otherwise, whitish colours represent the neutral regions (unlikely to position either of the tendencies). Except for 1 and 2, others change their chemical tendencies rather arbitrarily and consecutively over the molecular planes. This is especially apparent regarding those

with large structure and complicated functionalisation, e.g. 6-10 and 12-15. From theoretical argument, these molecules are more flexible when physically interacting with external complex structures; in other words, the molecular atoms and functionals can alter their roles rather flexibly according to their in-contact external ones.

Docking-based inhibibility

The results from docking technique provide the inhibitory properties of each bioactive compounds in the view of specific complex structures. This monitors the static interactions between the ligands (1-15) and their targeted proteins (3W37 and PTP1B).

Figure 5 highlights the most susceptible sites of the targeted proteins and Table 4 provides the corresponding primary docking parameters; the control drug (D) is acarbose. In this stage, the total docking score (DS) values and the number of hydrogen-like bonds are selected as the main indicators for inhibitory effectiveness. The former corresponds to pseudo values for Gibbs free energy of the inhibition and the latter represents strong intermolecular bonding. Overall, different compounds exhibit different tendencies towards the protein sites (either DS values or number of hydrophilic interactions). On average, the most effective inhibitors against 3W37 (α -glucosidase) are predicted into the order: 10 \approx 11 (DS -11.7 kcal.mol⁻¹) \approx 3 (DS -11.6 kcal.mol⁻¹) > 7 \approx 12 \approx D (DS -11.1 kcal.mol⁻¹). These candidates are expected to perform equal-to-elevated inhibitory effects towards α -glucosidase compared to the commercialised drug acarbose. This is of importance since biological inhibition in-reality is seldom activated towards a specific site but under inhibitory processes of simultaneity, in other words multi-site inhibition. Although possessing time- and cost-efficient advantages in drug discovery, the noticeable drawback of molecular docking technique refers to its algorithm based on static interaction. In suggestion, the ligand-protein kinetics and affinities can be assessed computationally using molecular dynamics simulations or measured experimentally using surface plasmon resonance technique.

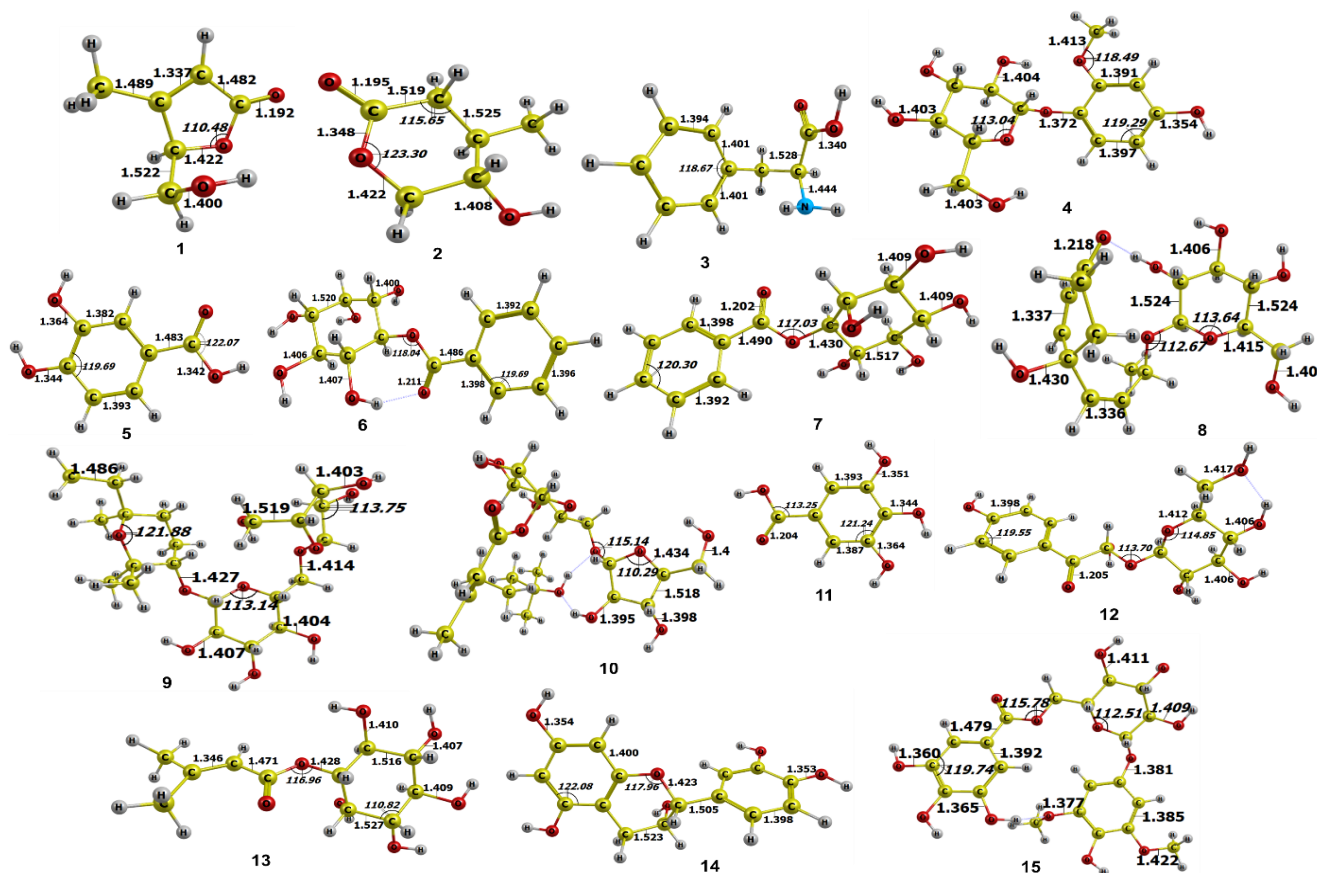
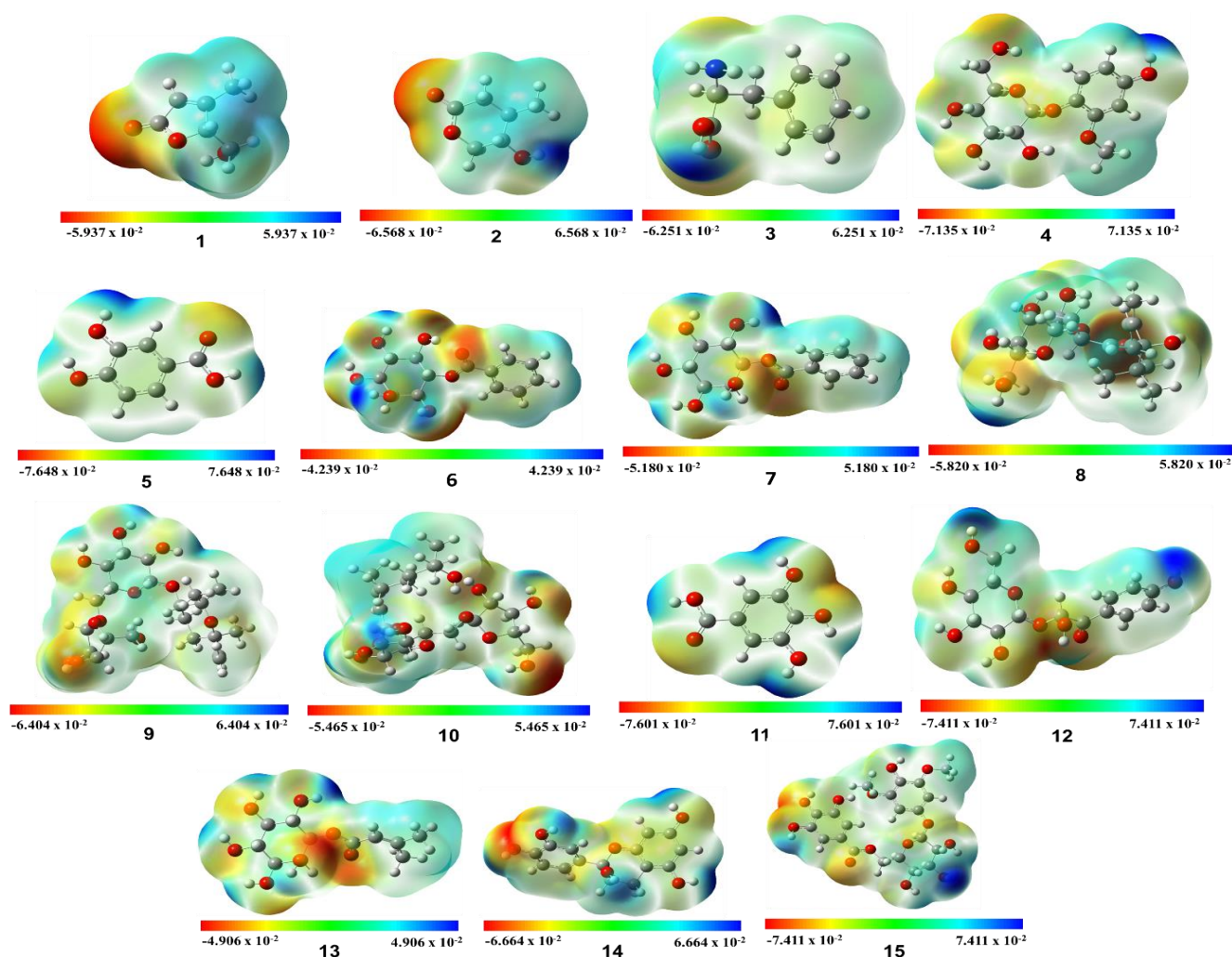


Figure 3: Geometrically optimised structures of 1-15 by DFT at level of theory M052X/6-311++(d,p)

Table 3: Ground state electronic energy and dipole moment values of 1-15 calculated by DFT at level of theory M052X/6-311++g(d,p)

Compound	Ground state electronic energy (a.u.)	Dipole moment (Debye)
1	-459.19816	5.039
2	-460.41187	5.241
3	-554.89303	1.632
4	-1108.18945	4.240
5	-571.38177	0.792
6	-1031.80267	1.549
7	-1031.80099	2.632
8	-1226.11216	2.480
9	-1650.20098	2.617
10	-1724.91438	6.370
11	-646.61688	0.905
12	-1221.55157	6.381
13	-956.76093	3.002
14	-1031.55060	3.045
15	-1792.90983	8.466

**Figure 4:** Molecular electrostatic potential (MEP) formed by mapping of total density over the electrostatic potential of 1-15 by DFT at level of theory M052X/def2-TZVPP

On the other side, the corresponding ligand-PTP1B order is: 11 (DS -12.0 kcal.mol⁻¹) > 13 (DS -11.8 kcal.mol⁻¹) > 5 (DS -11.2 kcal.mol⁻¹) > 3 (DS -11.0 kcal.mol⁻¹); besides, those with DS < -10.1 (referenced to D) can be considered as promising. However, it is noteworthy that this prediction solely is considered incomplete since it is only based on the assumption that the potential inhibitors are already placed in-contact with the targeted protein. If also regarding the dipole moment (representative of bio-medium compatibility), 10, 12, and 13 seem to be the most promising bio-inhibitors particularly. Although 11 can be profoundly interested from the view of static inhibibility, its in-practice applicability is likely to be resisted by the significantly low dipole moment. For further discussion, in-bold inhibitory systems, aka. the most effective ones, are selected.

Table 5 and Table 6 summarise the in-detail data of ligand-3W37 and ligand-PTP1B, respectively; Figure 6 and Figure 7 give the corresponding visualisations of in-site arrangements and interaction maps. By the theoretical interpretation, the most effective ligand-3W37 inhibitory structures are in the order: 11-3W37 (DS -13.7 kcal.mol⁻¹; RMSD 0.51 Å) > 10-3W37 (DS -13.2 kcal.mol⁻¹; RMSD 1.87 Å) > 3-3W37 (DS -13.1 kcal.mol⁻¹; RMSD 1.23 Å). If relatively comparing to those validated by bio-assays on α -glucosidase, these figures apparently correlate to high inhibitory effectiveness with assaying-based IC₅₀ values < 50 μ M (control drug IC₅₀ ca. 200 μ M).^{22,23} To some further extent, 15-3W37 (DS -12.8 kcal.mol⁻¹; RMSD 1.17 Å) > 12-3W37 (DS -12.6 kcal.mol⁻¹; RMSD 1.16 Å) \approx 5-3W37 (DS -12.5 kcal.mol⁻¹; RMSD 0.92 Å) > 8-3W37 (DS -12.4 kcal.mol⁻¹; RMSD 1.15 Å) can also be considered effective as the corresponding IC₅₀ values might correlate to the range under 100 μ M. Root-mean-square deviation (RMSD) is the difference of the average distance between backbone atoms of the protein sites before and after re-docking iterations, thus can represent bio-conformational rigidity of the protein or ligand-protein fitting. From this view, 11 can be thought having significantly high complementarity with the in-pose features of 3W37, thus deserved consideration of molecular modification in order to increase its dipole moment. In terms of ligand-PTP1B, the complexes can be arranged into the order: 11-PTP1B \approx 13-PTP1B > 5-PTP1B > 3- \approx 6- \approx 8- \approx 10- \approx 15-PTP1B. It is noteworthy that the PTP1B-based argument is considered as purely theoretical since to the best of our knowledge there has been no attempts

for experiment-theory correlation regarding tyrosine phosphatase 1B. Furthermore, 11 is predicted with as the most effective inhibitors against both 3W37 and PTP1B. Regarding the former, it seems to have special affinities towards arginine 676 in site 2. In terms of the latter, arginine 24 in site 1 is likely to be highly susceptible to the ligand. This approach of argument might provide the very first clues on promising amino acid residues to be targeted when designing drugs, especially using molecular dynamics techniques. The descriptive specification is provided by 2D projections, including hydrogen-like bonding (dashed arrow), van de Waals interaction (blurry purple), and conformational fitness (dashed contour). Given 3D in-pose morphology, the sites are rather open and spacious, cf. the ligands, suggesting the potentiality of modification/functionalization on current leading frameworks for better compatibility.

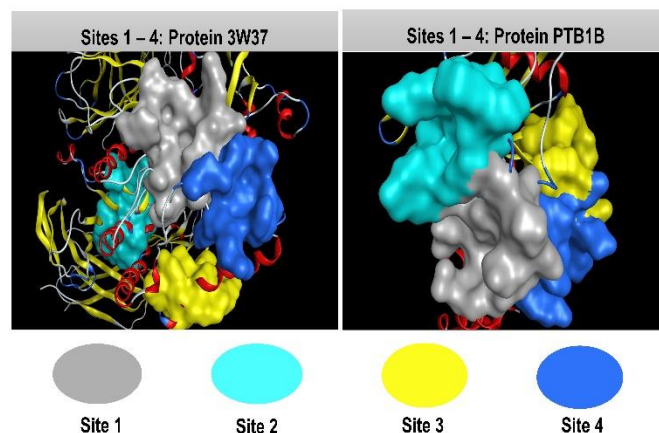


Figure 5: Quaternary structures of protein 3W37 and PTB1B with the approachable sites by 1-15 and the controlled drug Acarbose (D): site 1 (gray), site 2 (cyan), site 3 (yellow), site 4 (blue)

Table 4: Prescreening results on inhibibility of ligands (1-15) and controlled drug (D) towards the sites of proteins 3W37 and PTP1B

P	C	Site 1		Site 2		Site 3		Site 4		Average
		E	N	E	N	E	N	E	N	
3W37	1	-9.9	2	-8.2	1	-7.0	0	-7.3	0	-8.1
	2	-11.7	4	-9.1	2	-9.0	2	-8.4	1	-9.6
	3	-13.1	6	-10.5	3	-11.9	4	-10.7	3	-11.6
	4	-11.3	4	-8.4	1	-9.9	2	-10.0	2	-9.9
	5	-10.3	3	-12.5	6	-10.1	3	-9.9	2	-10.7
	6	-10.5	3	-9.4	2	-9.7	2	-12.2	5	-10.5
	7	-11.0	3	-10.3	2	-10.8	3	-12.7	6	-11.2
	8	-12.4	5	-9.0	2	-9.2	2	-8.3	1	-9.7
	9	-12.1	5	-9.0	2	-10.2	3	-9.4	2	-10.2
	10	-13.2	7	-10.9	3	-11.5	4	-11.1	3	-11.7
	11	-10.8	4	-13.7	7	-11.0	3	-11.2	3	-11.7
	12	-10.8	3	-12.6	6	-11.0	3	-9.8	2	-11.1
	13	-12.1	5	-10.8	3	-9.2	2	-9.0	2	-10.3
	14	-11.7	4	-8.8	2	-8.0	1	-8.1	1	-9.2
	15	-9.3	2	-9.8	3	-8.9	2	-12.8	5	-10.2
D	-10.9	3	-13.8	5	-10.9	3	-9.0	2	-11.2	
PTP1B	1	-11.9	5	-11.2	3	-10.1	2	-9.9	2	-10.8

2	-12.1	5	-10.9	3	-11.2	3	-9.4	2	-10.9
3	-10.7	3	-11.0	3	-12.7	6	-9.5	2	-11.0
4	-12.3	5	-8.8	2	-10.0	3	-9.1	2	-10.1
5	-13.4	7	-9.7	3	-11.8	4	-10.0	3	-11.2
6	-12.6	6	-8.9	2	-9.9	3	-8.3	2	-9.9
7	-12.7	5	-8.5	2	-8.9	2	-7.7	1	-9.5
8	-8.6	2	-9.0	2	-12.9	5	-10.9	3	-10.4
9	-10.9	3	-9.2	2	-10.9	3	-12.4	6	-10.9
10	-12.5	6	-10.4	3	-10.8	3	-9.7	2	-10.9
11	-13.8	8	-11.8	4	-11.2	3	-11.0	3	-12.0
12	-12.3	6	-9.0	2	-10.5	3	-9.4	2	-10.3
13	-10.9	3	-11.6	4	-11.0	3	-13.7	7	-11.8
14	-8.0	1	-9.1	2	-11.0	3	-7.9	1	-9.0
15	-12.7	5	-10.7	2	-10.3	3	-9.4	2	-10.8
D	-11.8	5	-10.3	3	-9.4	2	-9.0	2	-10.1

P: Protein; C: Compound; E: DS value (kcal.mol⁻¹); N: Number of hydrophilic interactions

Table 5: Molecular docking simulation results for ligands-3W37 inhibitory complexes

Ligand-protein complex			Hydrogen bond					van der Waals interaction		
Name	DS	RMSD	L	P		T	D	E		
1-3W37	-9.9	1.28	O	O	Asp 357	H-donor	2.79	-3.8	Asp 568, Phe 601, Arg 624, Trp 565, Asp 469, Met 470, Trp 329, Ile 396, Ile 358, Trp 467, Trp 432, Arg 552	
			O	N	His 626	H-acceptor	3.26	-0.7		
2-3W37	-11.7	0.78	O	O	Asp 568	H-donor	2.78	-2.3	His 626, Trp 329, Trp 432, Asp 469, Trp 467, Arg 552, Asp 357, Phe 601, Ile 396, Ile 358	
			C	S	Met 470	H-donor	3.71	-0.8		
			C	O	Asp 568	H-donor	3.37	-0.7		
			C	S	Met 470	H-donor	3.90	-0.7		
3-3W37	-13.1	1.23	N	S	Met 470	H-donor	3.82	-6.8	Gly 567, Arg 552, Trp 467, Ile 396, Trp 565, Phe 601, Asp 357, Trp 329, Asp 232	
			O	N	His 626	H-acceptor	3.14	-4.4		
			N	O	Asp 469	ionic	2.81	-5.9		
			N	O	Asp 469	ionic	3.48	-2.0		
			N	O	Asp 568	ionic	3.81	-0.9		
			6-ring	C	Trp 432	π -H	3.57	-0.7		
4-3W37	-11.3	0.99	O	O	Asp 357	H-donor	2.71	-3.4	Ala 628, Met 470, Asp 469, Arg 552, Gly 567, Trp 565, Asp 232, His 626, Ile 366, Trp 467, Trp 329, Phe 601	
			O	O	Asp 357	H-donor	3.00	-1.8		
			O	O	Asp 568	H-donor	2.86	-1.3		
			O	N	Trp 432	H-acceptor	2.89	-1.3		
5-3W37	-12.5	0.92	O	O	Glu 792	H-donor	2.77	-1.6	Leu 793, Gly 791, Thr 662, Glu 301, Asp 666, Leu 663, Gly 698, Tyr 659, Asn 758	
			O	O	Ile 759	H-donor	2.89	-1.0		
			O	N	Arg 699	H-acceptor	2.89	-0.9		
			O	N	Arg 676	ionic	3.08	-3.9		
			O	N	Arg 676	ionic	3.42	-2.2		
			O	N	Arg 670	ionic	3.14	-3.6		
6-3W37	-12.2	1.39	O	O	Asp 359	H-donor	3.19	-2.1	Met 361, Asp 362, Phe 364, His 373, Phe 374, Ala 363, Tyr 331	
			O	O	Asp 359	H-donor	2.85	-2.5		
			O	O	Asp 370	H-donor	3.15	-1.0		
			O	N	Arg 629	H-acceptor	2.96	-2.1		

			6-ring	C	Arg 332	π -H	4.67	-0.6	
7-3W37	-12.7	1.56	O	O	Asp 359	H-donor	3.05	-3.2	Arg 629, Phe 364, Ala 363
			O	O	Arg 332	H-donor	2.91	2.0	
			O	O	Tyr 331	H-donor	2.94	-1.9	
			C	5-ring	His 373	H- π	3.25	-1.0	
			C	5-ring	His 373	H- π	3.59	-0.6	
			O	5-ring	His 373	H- π	3.02	-1.5	
8-3W37	-12.4	1.15	O	O	Asp 232	H-donor	3.02	-1.1	Trp 467, Phe 601, Trp 432, Arg 552, Trp 329, Phe 476, Ile 396, Ile 358, His 626
			O	O	Asp 357	H-donor	3.10	-2.0	
			O	O	Asp 469	H-donor	2.71	-1.3	
			O	S	Met 470	H-donor	2.93	-0.7	
			C	O	Asp 568	H-donor	3.36	-0.7	
9-3W37	-12.1	1.36	C	O	Asp 568	H-donor	3.22	-0.9	Trp 329, Phe 601, Ile 396, His 626, Trp 565, Trp 467, Met 470, Gly 567, Trp 432, Phe 236, Phe 476, Arg 552, Lys 506, Ser 474, Asn 475, Asp 232
			C	O	Asp 568	H-donor	3.02	-1.6	
			O	O	Asp 357	H-donor	2.66	-2.4	
			O	O	Asp 568	H-donor	2.90	-1.6	
			O	O	Asp 469	H-donor	2.60	-2.3	
10-3W37	-13.2	1.87	C	O	Asp 568	H-donor	3.39	-1.0	Asp 469, Ser 474, Ile 396, Trp 432, Phe 236, Asp 398, Arg 552, Ile 358, Phe 601, Asn 475, Ala 628
			C	O	Asp 357	H-donor	3.28	-1.1	
			O	S	Met 470	H-donor	2.58	-1.0	
			O	O	Asp 568	H-donor	2.93	-2.2	
			O	N	Lys 506	H-acceptor	2.98	-6.3	
			C	6-ring	Trp 329	H- π	3.01	-0.9	
			C	6-ring	Phe 476	H- π	3.70	-0.7	
11-3W37	-13.7	0.51	O	O	Glu 792	H-donor	2.69	-3.7	Leu 663, Glu 301, Asp 666, Arg 699, Tyr 665, Gly 791, Thr 662, Gly 698
			O	O	Glu 792	H-donor	2.63	-5.1	
			O	N	Arg 670	H-acceptor	3.04	-1.2	
			O	N	Arg 670	ionic	3.04	-4.2	
			O	N	Arg 676	ionic	2.69	-6.9	
			O	N	Arg 676	ionic	3.15	-3.6	
			O	N	Arg 676	ionic	3.36	-2.5	
12-3W37	-12.6	1.16	O	O	Asn 758	H-donor	2.85	-2.8	Thr 662, Tyr 659, Arg 670, Gly 700, Thr 790, Glu 301, Val 760, Gly 791, Leu 663
			O	O	Ile 759	H-donor	2.91	-1.4	
			O	O	Ile 759	H-donor	2.83	-2.9	
			O	O	Glu 792	H-donor	3.03	-3.5	
			O	N	Glu 792	H-acceptor	2.82	-3.1	
			6-ring	C	Arg 699	π -H	3.03	-0.6	
13-3W37	-12.1	1.19	C	O	Asp 357	H-donor	3.30	-1.0	Ala 602, Trp 329, Phe 601, Ile 358, His 626, Ile 396, Arg 552, Asp 459, Trp 467, Trp 432, Trp 565, Asp 568
			O	O	Asp 357	H-donor	3.41	-0.6	
			O	O	Asp 357	H-donor	2.93	-3.3	
			O	S	Met 470	H-donor	3.60	-1.5	
			O	S	Met 470	H-donor	3.21	-1.7	
14-3W37	-11.7	0.59	O	O	Asp 630	H-donor	2.98	-4.0	Asp 568, Trp 432, Ile 369, Arg 552, Asp 469, Phe 601, Met 470, Ala 628, Glu 603, Thr 631, Ala 602
			O	O	Asp 357	H-donor	3.44	-0.6	
			C	5-ring	Trp 329	H- π	4.42	-0.6	
			C	5-ring	Trp 329	H- π	3.62	-0.6	

15-3W37	-12.8	1.17	O	O	Asp 359	H-donor	2.85	-2.0	Ala 363, Phe 364, Arg 332, Gly 330, Tyr 331, Phe 374, Asp 370, Val 372
			O	O	Asp 359	H-donor	2.92	-1.0	
			O	O	Asp 359	H-donor	3.27	-0.9	
			O	O	Arg 629	H-donor	3.04	-1.5	
			C	5-ring	His 373	H- π	3.42	-0.8	
D-3W37	-13.8	1.17	O	O	Glu 792	H-donor	3.20	-0.7	Glu 301, Phe 680, Arg 814, Thr 681, Gly 698, Leu 663, Gly 700, Asn 758, Thr 790, Tyr 659, Val 760, Gly 791, Asp 666, Arg 670, Thr 299, Pro 683
			O	O	Ile 759	H-donor	2.77	-2.1	
			O	N	Arg 699	H-acceptor	2.77	-4.4	
			O	N	Arg 699	H-acceptor	3.23	-1.7	
			O	N	Arg 676	H-acceptor	2.99	-0.6	

DS: Docking score energy (kcal.mol⁻¹); RMSD: Root-mean-square deviation (Å); L: Ligand; P: Protein; T: Type; D: Distance (Å); E: Energy (kcal.mol⁻¹)

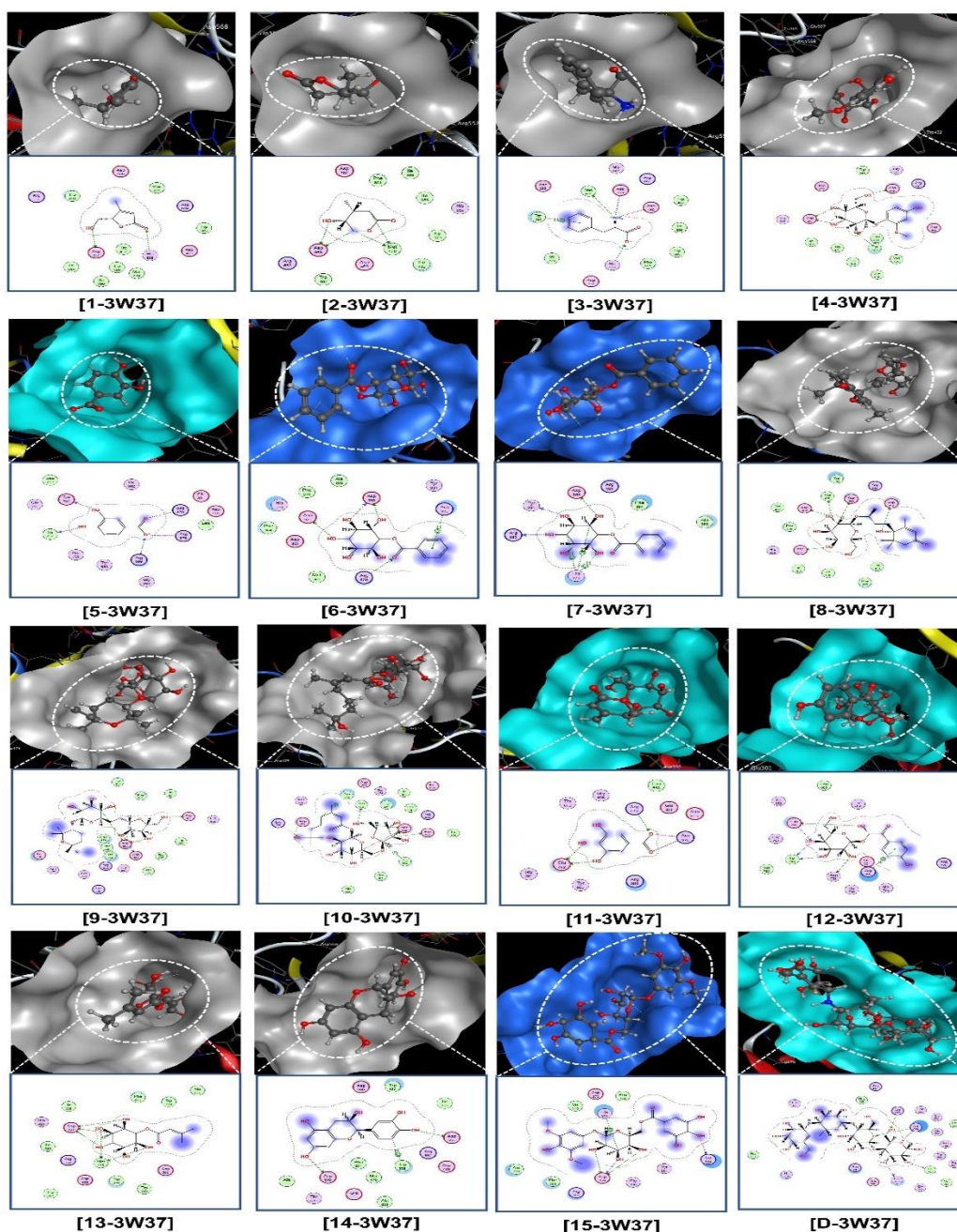


Figure 6: Visual presentation and in-pose interaction map of ligand-3W37 inhibitory structures

QSARIS-based physicochemical properties

Table 7 summarises the physicochemical properties of the compounds (retrieved from QSARIS system) and the number of hydrogen bonds (counted from docking-based results). Referencing to Lipinski's criteria, all the compounds are considered suitable for biocompatible applications in general and development of oral-intake drugs in particular, i.e. (i) molecular mass < 500 amu; (ii) $\log P < 2$; (iii) total hydrogen-like counts < 5 (either donating or accepting). Given polarisability, 10 (70.8 Å³) and 15 (64.7 Å³), already predicted promising by quantum calculation and docking simulation, also possess the values of most significance (along with that of 9); on the other side, 11 is again considered unfavoured for biological applications given by its low polarisability (19.1 Å³). This property, by definition, represents the sensitivity to external electric fields, such as those are created by other polarised components (e.g. amino-acid-based protein structures) or by the solvation double layers. The unit conversion is given by Clausius-Mossotti relation: $10^6/4\pi\epsilon_0 [A^2 \cdot s^4 \cdot kg^{-1}] \equiv 1 [cm^3]$.³⁷ From the point of octanol/water partition coefficients ($\log P$), 11 is also unconvincing to its aqueous transportability given the relatively higher figure than others.

ADMET-based pharmacokinetics and pharmacology

The ADMET properties of the compounds are separated into Table 8 (1-8) and Table 8 (9-15 and D), including chemical absorption, distribution, metabolism, excretion, and toxicity. Overall, all the compounds are predicted highly safe for use in humans. Regarding toxicity: (i) almost no mutagenic potentials (except for 14); (ii) almost no potential for fatal ventricular arrhythmia as hERG inhibitors (except for 9); (iii) almost no potential for hepatotoxicity (except for 3); (iv) no skin sensitisation; (v) toxicity to bacterium *T. Pyriformis* (pIGC50 > -0.5 log µg.L⁻¹ yet no effects against fish Flathead Minnows (LC50 > -0.3). Regarding excretion, all the compounds are predicted not under the disposition (renal clearance) by Organic Cation Transporter 2. Regarding metabolism, no potential interaction (either as inhibitors or substrates) to the cytochromes P450 family, indicating that they are not oxidised by the liver and might remain a longer span in the body. Regarding distribution, all the compounds are plasma-tissue balanced (-0.15 < log VDss < 0.45), less likely to cross the blood-brain barrier (logBB < 0), and unable to affect the central nervous system (log PS <

-3). Regarding absorption, no significant interaction with P-glycoprotein is predicted, thus no effects to the extrusion of the toxins and xenobiotics out of cells. However, except for 1 and 2 (> 90 %), the compounds in general register low-to-moderate intestinal absorbability, especially the most promising candidates 10 (17.936 %), 12 (25.796 %), and 15 (26.225 %). Therefore, the candidates might require certain special prescription in order to increase the absorbability.

Conclusion

This is the first theory-based study for screening of antidiabetic potentiality against α -glucosidase (PDB-3W37) and tyrosine phosphatase 1B (UniProtKB-PTP1B) of undetermined bioactive components (1-15) extracted from *Euonymus laxiflorus*. Dipole moment values indicate the favoured bio-medium compatibility of 10 (6.370 Debye), 12 (6.381 Debye), and 15 (8.446 Debye), while exclude the potential of 5 (0.792 Debye) and 11 (0.905 Debye). Molecular electrostatic potential maps imply the intermolecular interacting flexibility of 6-10 and 12-15. Docking-based simulation predicts the most effective ligand-3W37 inhibitory systems to the order: 11-3W37 (DS -13.7 kcal.mol⁻¹; RMSD 0.51 Å) > 10-3W37 (DS -13.2 kcal.mol⁻¹; RMSD 1.87 Å) > 3-3W37 (DS -13.1 kcal.mol⁻¹; RMSD 1.23 Å) > 15-3W37 (DS -12.8 kcal.mol⁻¹; RMSD 1.17 Å) > 12-3W37 (DS -12.6 kcal.mol⁻¹; RMSD 1.16 Å) \approx 5-3W37 (DS -12.5 kcal.mol⁻¹; RMSD 0.92 Å) > 8-3W37 (DS -12.4 kcal.mol⁻¹; RMSD 1.15 Å). Given polarisability, 10 (70.8 Å³) and 15 (64.7 Å³) are considered highly suitable for bio-inhibitory applications; meanwhile, 11 (19.1 Å³) is especially discouraged. Other physicochemical properties justify the drug-likeness of all candidates. Besides low intestinal absorbability, all the compounds are expected to have favourable pharmacokinetics and pharmacology. Altogether, the theoretical screening specifies 10 (7-Hydroxy-6,7-dihydro-cis/trans-geraniate, 3-O- α -L-arabinopyranosyl (1 \rightarrow 6)- β -D-glucopyranosyl) and 15 (3,5-dimethoxy-4-hydroxyphenol)-1-O- β -D-(6'-O-galloyl)-glucopyranoside) as the most antidiabetic compounds from *E. laxiflorus* methanol extract, thus deserved further experimental attempts for cumulative isolation and bioassay trials.

Table 6: Molecular docking simulation results for ligands-PTP1B inhibitory complexes

Ligand-protein complex			Hydrogen bond				van der Waals interaction		
Name	DS	RMSD	L	P	T	D	E		
1-PTP1B	-11.9	1.05	O	O	Asp 48	H-donor	2.92	-0.8	Gly 259, Ile 219, Gln 262, Tyr 20, Ile 261
			O	S	Met 258	H-donor	3.42	-0.8	
			O	N	Arg 24	H-acceptor	3.12	-2.0	
			O	N	Arg 254	H-acceptor	3.18	-2.9	
			O	N	Arg254	H-acceptor	3.40	-1.0	
2- PTP1B	-12.1	1.17	O	S	Met 258	H-donor	3.35	-1.5	Tyr 20, Gly 259, Ile 219, Asp 48
			O	N	Gln 262	H-acceptor	3.06	-1.0	
			O	N	Arg 24	H-acceptor	3.12	-0.8	
			O	N	Arg 254	H-acceptor	3.34	-0.8	
			O	N	Arg 254	H-acceptor	2.98	-3.6	
3- PTP1B	-12.7	1.87	N	O	Ser 205	H-donor	2.70	-1.2	Pro 210, Leu 204, Pro 206, Ser 203, Gln 78
			N	O	His 208	H-donor	2.80	-1.8	
			N	O	Gly 209	H-donor	2.77	-2.8	
			O	N	Val 211	H-acceptor	2.76	-4.8	
			O	N	Arg 79	ionic	3.50	-1.9	
6-ring	C	Ser 80	π -H	3.72	-0.8				
4- PTP1B	-12.3	1.06	O	S	Met 258	H-donor	3.35	-1.7	

			O	O	Asp 48	H-donor	3.08	-1.0	His 25, Ser 28, Arg 254, Gly 259, Ile 219, Val 49
			O	O	Arg 24	H-donor	2.98	-1.0	
			O	N	Arg 24	H-acceptor	3.20	-2.3	
			O	N	Gln 262	H-acceptor	3.18	-0.6	
5- PTP1B	-13.4	1.24	O	O	Asp 48	H-donor	2.99	-1.7	Tyr 20, Met 258, Val 49, Ile 219, Ile 261, Gly 259
			O	N	Arg 254	H-acceptor	2.91	-6.8	
			O	N	Arg 24	H-acceptor	3.00	-3.1	
			O	N	Arg 254	H-acceptor	3.21	-3.8	
			O	N	Gln 262	H-acceptor	3.20	-0.7	
			O	N	Arg 24	ionic	3.73	-1.1	
			O	N	Arg 24	ionic	3.33	-2.6	
6- PTP1B	-12.6	1.47	C	S	Met 258	H-donor	3.02	-0.9	Asp 48, Val 49, Gly 259, Ala 27
			O	O	Ser 28	H-donor	3.11	-1.0	
			O	O	Asp 29	H-donor	3.00	-1.9	
			O	N	Arg 24	H-acceptor	3.34	-0.8	
			O	N	Gln 262	H-acceptor	3.34	-1.0	
			O	N	Arg 254	H-acceptor	3.13	-1.5	
7- PTP1B	-12.7	1.21	O	O	Asp 48	H-donor	2.97	-1.5	Ser 28, Ala 27, Asp 29, Arg 254, Ile 219, Gly 259, Val 449
			O	S	Met 258	H-donor	3.11	-2.4	
			O	N	Arg 24	H-acceptor	3.23	-1.0	
			O	N	Arg 24	H-acceptor	3.19	-1.0	
			O	N	Gln 262	H-acceptor	3.06	-0.8	
8- PTP1B	-12.9	1.90	O	O	Leu 204	H-donor	2.41	1.5	Gln 102, Glu 207, Gly 209, Pro 210, Leu 71, Ser 80, Met 74, Arg 79, Glu 75, Gln 78
			O	O	Gln 78	H-donor	3.00	-1.7	
			O	C	Pro 210	H-acceptor	3.11	-0.8	
			O	N	Val 211	H-acceptor	3.04	-1.7	
			O	N	Arg 79	H-acceptor	2.92	-3.4	
9- PTP1B	-12.4	1.62	O	O	Glu 76	H-donor	2.77	-4.0	Val 244, Asp 245, Leu 234, Val 249, Leu 251, Lys 255
			C	O	Glu 252	H-donor	3.45	-0.8	
			O	O	Ser 243	H-donor	3.23	-1.7	
			O	C	Lys 248	H-acceptor	3.25	-1.2	
			O	C	Lys 248	H-acceptor	3.01	-1.1	
			O	N	Arg 238	H-acceptor	2.91	-3.7	
10- PTP1B	-12.5	1.72	C	S	Met 258	H-donor	3.53	-0.9	Ser 28, Phe 30, Asp 29, Pro 31, Lys 36, Asp 48, Gly 259, Tyr 20
			O	O	Gln 262	H-donor	2.96	-1.3	
			O	N	Arg 254	H-acceptor	3.01	-1.9	
			O	N	Arg 24	H-acceptor	3.01	-2.2	
			O	N	Gln 262	H-acceptor	3.13	-1.2	
			O	C	Cys 32	H-acceptor	3.27	-1.3	
11- PTP1B	-13.8	1.44	O	O	Asp 48	H-donor	2.97	-3.4	Tyr 20, Gly 259, Met 258, Ile 219, Val 49
			O	O	Asp 48	H-donor	3.05	-2.3	
			O	N	Arg 254	H-acceptor	2.84	-4.6	
			O	N	Arg 24	H-acceptor	3.34	-1.7	
			O	N	Arg 254	H-acceptor	3.58	-0.6	
			O	N	Gln 262	H-acceptor	3.02	-2.7	
			O	N	Arg 24	ionic	3.25	-3.0	

			O	N	Arg 24	ionic	3.10	-3.8	
12- PTP1B	-12.3	1.06	O	O	Asp 29	H-donor	2.95	-1.6	Gly 259, Val 49, Gln 262, Phe 30, Phe 52, Ala 27, Arg 24, Ile 219
			O	O	Asp 29	H-donor	2.87	-3.8	
			O	O	Ser 28	H-donor	2.94	-1.9	
			O	O	Asp 48	H-donor	3.00	-1.0	
			O	S	Met 258	H-donor	3.51	-1.8	
			O	N	Arg 254	H-acceptor	3.23	-1.0	
13- PTP1B	-13.7	1.81	C	O	Ser 243	H-donor	3.46	-0.6	Gly 252, Val 249, Val 244, Lys 248, Leu 234
			O	O	Glu 76	H-donor	2.80	-1.7	
			O	O	Ser 243	H-donor	2.88	-1.2	
			O	O	Glu 76	H-donor	3.15	-2.0	
			O	N	Arg 238	H-acceptor	3.14	-1.1	
			O	N	Arg 238	H-acceptor	2.81	-3.3	
			O	N	Asp 245	H-acceptor	2.77	-2.9	
14- PTP1B	-11.0	0.51	O	O	His 208	H-donor	2.82	-1.1	Met 74, Arg 79, Ser 80, Pro 210, Gly 209, Ser 205, Lys 73, Glu 75
			6-ring	N	Gln 78	π -H	3.70	-0.7	
			6-ring	C	Pro 206	π -H	3.80	-0.6	
15- PTP1B	-12.7	1.51	O	S	Met 258	H-donor	3.82	-0.9	Gly 259, Asp 48, Gln 262, Val 49, Ala 27, Phe 52, Lys 36, Phe 30, Cys 32, Arg 254, His 25, Ile 219, Ser 28
			O	S	Met 258	H-donor	3.32	-0.1	
			O	O	Asp 29	H-donor	3.08	-3.0	
			C	S	Met 258	H-donor	3.79	-1.0	
			O	N	Arg 24	H-acceptor	2.95	-3.2	
D-PTP1B	-11.8	1.62	O	O	Arg 24	H-donor	2.87	-1.8	Asp48, Met 258, Arg 254, Gln 21, Phe 52, Phe 30, Ser 28, Cys 32, Lys 38
			O	O	Arg 24	H-donor	3.02	-1.7	
			O	O	Asp 29	H-donor	3.22	-2.0	
			O	O	Asp 29	H-donor	3.06	-0.9	
			O	N	His 25	H-acceptor	3.28	-1.4	

DS: Docking score energy (kcal.mol⁻¹); RMSD: Root-mean-square deviation (Å); L: Ligand; P: Protein; T: Type; D: Distance (Å); E: Energy (kcal.mol⁻¹)

Table 7: Physicochemical properties of studied ligands (1-15 and D)

Ligand (Compound)	Mass (amu)	Polarizability (Å ³)	Volume (Å ³)	Dispersion coefficients		Hydrogen bond (3W37/PTP1B)	
				LogP	LogS	H-acceptor	H-donor
1	128.1	18.6	180.5	-0.18	-0.47	1/3	1/1
2	130.1	19.3	192.1	0.12	-0.23	0/4	4/1
3	165.3	25.8	228.9	1.01	-1.34	1/1	1/3
4	302.1	41.1	346.3	-1.23	-0.49	1/2	3/3
5	154.2	18.4	182.5	1.12	-0.89	1/4	2/1
6	284.4	39.7	321.9	-1.25	-0.90	1/3	3/3
7	284.2	39.8	376.4	-1.24	-0.90	0/3	3/2
8	386.2	50.7	482.9	-1.34	-0.80	0/3	5/2
9	464.3	71.0	502.0	-0.74	-1.21	0/3	5/3
10	478.4	70.8	503.4	-1.98	-1.16	1/4	3/2
11	170.2	19.1	191.4	0.85	-0.53	1/4	2/2
12	344.1	43.7	387.2	-1.78	-0.51	1/1	4/5
13	262.0	37.3	307.2	-2.22	-0.29	0/3	5/4

14	290.2	40.5	302.7	1.98	-1.74	0/0	2/1
15	484.1	64.7	515.9	-0.68	-1.21	0/1	4/4
D	645.6	55.8	658.7	-7.26	1.47	3/1	2/4

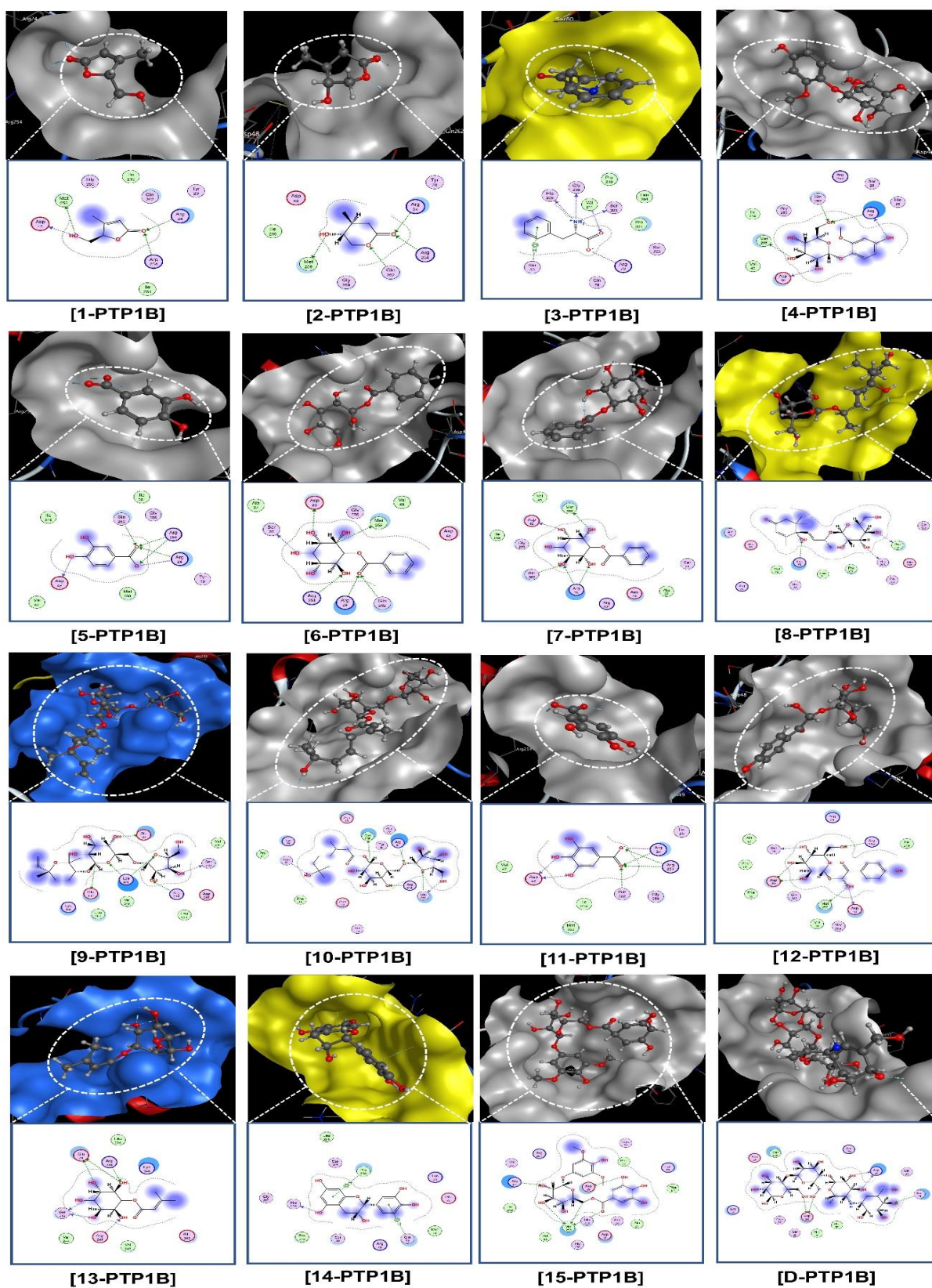


Figure 7: Visual presentation and in-pose interaction map of ligand-PTB1B inhibitory structures

Table 8: Pharmacokinetic and pharmacological properties of compounds 1-8

Property	1	2	3	4	5	6	7	8	Unit
Absorption									
Water solubility	0.145	0.074	-2.89	-1.389	-2.069	-1.459	-1.459	-2.613	(1)
Caco2 permeability	1.151	1.157	0.62	0.206	0.49	0.163	0.163	0.379	(2)
Intestinal absorption (human)	94.241	94.266	76.21	40.502	71.174	22.404	22.404	47.786	(3)
Skin Permeability	-4.03	-4.002	-2.734	-2.762	-2.727	-2.754	-2.754	-2.859	(4)
P-glycoprotein substrate	No	No	No	Yes	No	No	No	Yes	(5)
P-glycoprotein I inhibitor	No	(5)							
P-glycoprotein II inhibitor	No	(5)							
Distribution									
VDss (human)	-0.106	-0.121	-0.326	0.076	-1.298	-0.516	-0.516	-0.131	(6)
Fraction unbound (human)	0.771	0.764	0.492	0.702	0.648	0.51	0.51	0.601	(6)
BBB permeability	-0.264	-0.279	-0.271	-1.088	-0.683	-1.176	-1.176	-1.067	(7)
CNS permeability	-2.923	-2.869	-2.675	-3.941	-3.305	-4.631	-4.631	-3.632	(8)
Metabolism									
CYP2D6 substrate	No	(5)							
CYP3A4 substrate	No	(5)							
CYP1A2 inhibitor	No	(5)							
CYP2C19 inhibitor	No	(5)							
CYP2C9 inhibitor	No	(5)							
CYP2D6 inhibitor	No	(5)							
CYP3A4 inhibitor	No	(5)							
Excretion									
Total Clearance	0.661	0.219	0.452	0.584	0.551	0.3	0.3	1.389	(9)
Renal OCT2 substrate	No	(5)							
Toxicity									
AMES toxicity	No	(5)							
Max. tolerated dose (human)	1.14	1.189	0.935	0.564	0.814	0.711	0.711	1.095	(10)
hERG I inhibitor	No	(5)							
hERG II inhibitor	No	(5)							
Oral Rat Acute Toxicity (LD50)	1.833	1.849	2.193	1.821	2.423	2.265	2.265	2.2	(11)
Oral Rat Chronic Toxicity (LOAEL)	2.584	2.546	1.954	3.399	2.021	3.83	3.83	3.505	(12)
Hepatotoxicity	No	No	Yes	No	No	No	No	No	(5)
Skin Sensitisation	No	(5)							
<i>T.Pyriformis</i> toxicity	-0.864	-0.77	0.269	0.285	0.273	0.285	0.285	0.285	(13)
Minnow toxicity	2.815	2.82	2.247	4.793	2.451	2.823	2.823	4.926	(14)

(1) log mol.L⁻¹; (2) log Papp (10⁻⁶ cm.s⁻¹); (3) %; (4) log Kp; (5) Yes/No; (6) log L.kg⁻¹; (7) log BB; (8) log PS;

(9) log mL.min⁻¹.kg⁻¹; (10) log mg.kg⁻¹.day⁻¹; (11) mol.kg⁻¹; (12) log mg.kg⁻¹.bw.day⁻¹; (13) log µg.L⁻¹; (14) log mM

Table 9: Pharmacokinetic and pharmacological properties of compounds 9-15 and D

Property	9	10	11	12	13	14	15	D	Unit
Absorption									
Water solubility	-1.467	-1.4	-2.56	-0.594	-0.418	-3.179	-2.926	-1.482	(1)
Caco2 permeability	-0.332	0.479	-0.081	-0.497	-0.371	-0.292	-1.123	-0.481	(2)
Intestinal absorption (human)	26.015	17.936	43.374	25.796	15.842	73.244	26.225	4.172	(3)

Skin Permeability	-2.735	-2.735	-2.735	-2.742	-3.248	-2.736	-2.735	-2.735	(4)
P-glycoprotein substrate	Yes	Yes	No	No	No	Yes	Yes	Yes	(5)
P-glycoprotein I inhibitor	No	(5)							
P-glycoprotein II inhibitor	No	(5)							
Distribution									
VDss (human)	0.584	0.184	-1.855	0.323	-0.126	0.675	1.616	-0.836	(6)
Fraction unbound (human)	0.542	0.481	0.617	0.619	0.722	0.156	0.219	0.505	(6)
BBB permeability	-1.284	-1.238	-1.102	-1.338	-1.241	-1.017	-1.996	-1.717	(7)
CNS permeability	-5.189	-4.945	-3.74	-4.296	-4.64	-3.314	-4.392	-6.438	(8)
Metabolism									
CYP2D6 substrate	No	(5)							
CYP3A4 substrate	No	(5)							
CYP1A2 inhibitor	No	(5)							
CYP2C19 inhibitor	No	(5)							
CYP2C9 inhibitor	No	(5)							
CYP2D6 inhibitor	No	(5)							
CYP3A4 inhibitor	No	(5)							
Excretion									
Total Clearance	1.437	1.498	0.518	0.583	1.552	0.254	0.566	0.428	(9)
Renal OCT2 substrate	No	(5)							
Toxicity									
AMES toxicity	No	No	No	No	No	Yes	No	No	(5)
Max. tolerated dose (human)	0.571	0.354	0.7	0.353	1.183	0.542	0.415	0.435	(10)
hERG I inhibitor	No	(5)							
hERG II inhibitor	Yes	No	No	No	No	No	No	Yes	(5)
Oral Rat Acute Toxicity (LD50)	2.611	2.481	2.218	2.573	1.696	2.103	2.469	2.449	(11)
Oral Rat Chronic Toxicity (LOAEL)	3.846	4.102	3.06	5.004	3.665	2.759	3.689	5.319	(12)
Hepatotoxicity	No	(5)							
Skin Sensitisation	No	(5)							
T.Pyriformis toxicity	0.285	0.285	0.285	0.285	0.285	0.335	0.285	0.285	(13)
Minnow toxicity	6.252	3.935	3.188	3.775	3.249	1.947	7.293	16.823	(14)

(1) log mol.L⁻¹; (2) log Papp (10⁻⁶ cm.s⁻¹); (3) %; (4) log Kp; (5) Yes/No; (6) log L.kg⁻¹; (7) log BB; (8) log PS;

(9) log mL.min⁻¹.kg⁻¹; (10) log mg.kg⁻¹.day⁻¹; (11) mol.kg⁻¹; (12) log mg.kg⁻¹.bw.day⁻¹; (13) log µg.L⁻¹; (14) log mM

Conflict of Interest

The authors declare no conflict of interest.

Authors' Declaration

The authors hereby declare that the work presented in this article is original and that any liability for claims relating to the content of this article will be borne by them.

Acknowledgments

This research was funded by Tay Nguyen University [Grant No. T2022-41CBTD]. The authors also acknowledge the partial support from Hue University [Project No. DHH2022-01-198].

References

1. Abaira C, Colwell JA, Nuttall FQ, Sawin CT, Nagel NJ, Comstock JP, Emanuele N V, Levin SR, Henderson W, Lee

- HS. Veterans Affairs Cooperative Study on glycemic control and complications in type II diabetes (VA CSDM): results of the feasibility trial. *Diabetes Care*. 1995;18(8):1113–23.
2. Ohkubo Y, Kishikawa H, Araki E, Miyata T, Isami S, Motoyoshi S, Kojima Y, Furuyoshi N, Shichiri M. Intensive insulin therapy prevents the progression of diabetic microvascular complications in Japanese patients with non-insulin-dependent diabetes mellitus: a randomized prospective 6-year study. *Diabetes Res Clin Pract*. 1995;28(2):103–17.
3. Klein R, Klein BEK, Moss SE, Cruickshanks KJ. Relationship of hyperglycemia to the long-term incidence and progression of diabetic retinopathy. *Arch Intern Med*. 1994;154(19):2169–78.
4. Wu Y, Ding Y, Tanaka Y, Zhang W. Risk factors contributing to type 2 diabetes and recent advances in the treatment and prevention. *Int J Med Sci*. 2014;11(11):1185.
5. Sandholm N, Forsblom C. Genetics of Diabetic Microvascular Disease. *Microvasc Dis Diabetes*. 2020;23–44.

6. Draznin B, Aroda VR, Bakris G, Benson G, Brown FM, Freeman R, Green J, Huang E, Isaacs D, Kahan S. 2. Classification and Diagnosis of Diabetes: Standards of Medical Care in Diabetes-2022. *Diabetes Care*. 2022;45(Supplement_1):S17–38.
7. Henning RJ. Type-2 diabetes mellitus and cardiovascular disease. *Future Cardiol*. 2018;14(6):491–509.
8. Holman RR, Cull CA, Turner RC. A randomized double-blind trial of acarbose in type 2 diabetes shows improved glycemic control over 3 years (UK Prospective Diabetes Study 44). *Diabetes Care*. 1999;22(6):960–4.
9. Lebovitz HE. Alpha-glucosidase inhibitors. *Endocrinol Metab Clin North Am*. 1997;26(3):539–51.
10. Vieira MNN, Lyra e Silva NM, Ferreira ST, De Felice FG. Protein tyrosine phosphatase 1B (PTP1B): a potential target for Alzheimer's therapy? *Front Aging Neurosci*. 2017;9(7):Article ID 28197094.
11. Özil M, Emirik M, Etlik SY, Ülker S, Kahveci B. A simple and efficient synthesis of novel inhibitors of alpha-glucosidase based on benzimidazole skeleton and molecular docking studies. *Bioorg Chem*. 2016;68:226–35.
12. Nikookar H, Mohammadi-Khanaposhtani M, Imanparast S, Faramarzi MA, Ranjbar PR, Mahdavi M, Larjani B. Design, synthesis and in vitro α -glucosidase inhibition of novel dihydropyrano [3, 2-c] quinoline derivatives as potential anti-diabetic agents. *Bioorg Chem*. 2018;77:280–6.
13. Adelusi TI, Boyenle ID, Tolulope A, Adebisi J, Fatoki JO, Ukachi CD, Oyedele AQK, Ayoola AM, Timothy AA. GCMS fingerprints and phenolic extracts of *Allium sativum* inhibit key enzymes associated with type 2 diabetes. *J Taibah Univ Med Sci*. 2023;18(2):337.
14. Nguyen QV, Nguyen NH, Wang SL, Nguyen VB, Nguyen AD. Free radical scavenging and antidiabetic activities of *Euonymus laxiflorus* Champ. extract. *Res Chem Intermed*. 2017;43:5615–24.
15. Nguyen VB, Wang SL, Nguyen AD, Lin ZH, Doan CT, Tran TN, Huang HT, Kuo YH. Bioactivity-guided purification of novel herbal antioxidant and anti-NO compounds from *Euonymus laxiflorus* Champ. *Molecules*. 2018;24(1):120.
16. Kuo YH, Huang HC, Chiou WF, Shi LS, Wu TS, Wu YC. A Novel NO-Production-Inhibiting Triterpene and Cytotoxicity of Known Alkaloids from *Euonymus laxiflorus*. *J Nat Prod*. 2003;66(4):554–7.
17. Nguyen VB, Nguyen QV, Nguyen AD, Wang SL. Screening and evaluation of α -glucosidase inhibitors from indigenous medicinal plants in Dak Lak Province, Vietnam. *Res Chem Intermed*. 2017;43:3599–612.
18. Nguyen VB, Wang SL, Nguyen TH, Nguyen MT, Doan CT, Tran TN, Lin ZH, Nguyen QV, Kuo YH, Nguyen AD. Novel potent hypoglycemic compounds from *Euonymus laxiflorus* Champ. and their effect on reducing plasma glucose in an ICR mouse model. *Molecules*. 2018;23(8):1928.
19. Nguyen VB, Wang SL, Nguyen AD, Vo TPK, Zhang LJ, Nguyen QV, Kuo YH. Isolation and identification of novel α -amylase inhibitors from *Euonymus laxiflorus* Champ. *Res Chem Intermed*. 2018;44:1411–24.
20. Fan J, Fu A, Zhang L. Progress in molecular docking. *Quant Biol*. 2019;7(2):83–9.
21. Kapetanovic IM. Computer-aided drug discovery and development (CADD): In silico-chemico-biological approach. *Chem Biol Interact*. 2008;171(2):165–76.
22. Thao TTP, Bui TQ, Quy PT, Bao NC, Van Loc T, Van Chien T, Chi NL, Van Tuan N, Van Sung T, Nhung NTA. Isolation, semi-synthesis, docking-based prediction, and bioassay-based activity of *Dolichandrone* spathacea iridoids: new catalpol derivatives as glucosidase inhibitors. *RSC Adv*. 2021;11:11959–75.
23. Thi T, Thao P, Bui TQ, Thi N, Hai T, Huynh LK, Quy PT, Bao NC, Dung NT, Chi NL, Loc T Van, Smirmova IE, Petrova A V, Ninh PT, Sung T Van, Thi N, Nhung A. Newly synthesised oxime and lactone derivatives from *Dipterocarpus alatus* dipterocarpol as anti-diabetic inhibitors: experimental bioassay-based evidence and theoretical computation-based prediction. *RSC Adv*. 2021;11:35765–82.
24. Adelusi TI, Abdul-Hammed M, Idris MO, Kehinde OQ, Boyenle ID, Divine UC, Adedotun IO, Folorunsho AA, Kolawole OE. Exploring the inhibitory potentials of *Momordica charantia* bioactive compounds against Keap1-Kelch protein using computational approaches. *Silico Pharmacol*. 2021;9(1):39.
25. Adelusi TI, Abdul-Hammed M, Idris MO, Oyedele QK, Adedotun IO. Molecular dynamics, quantum mechanics and docking studies of some Keap1 inhibitors—An insight into the atomistic mechanisms of their antioxidant potential. *Heliyon*. 2021;7(6):e07317.
26. Adelusi TI, Oyedele AQK, Monday OE, Boyenle ID, Idris MO, Ogunlana AT, Ayoola AM, Fatoki JO, Kolawole OE, David KB. Dietary polyphenols mitigate SARS-CoV-2 main protease (Mpro)—Molecular dynamics, molecular mechanics, and density functional theory investigations. *J Mol Struct*. 2022;1250:131879.
27. Gaussian 09, Revision A.02, M. J. Frisch, G. W. Trucks, H. B. Schlegel, G. E. Scuseria, M. A. Robb, J. R. Cheeseman, G. Scalmani, V. Barone, G. A. Petersson, H. Nakatsuji, X. Li, M. Caricato, A. Marenich, J. Bloino, B. G. Janesko, R. Gomperts, B. Mennucci.
28. Markovi ZS, Dimitri JM. Mechanistic study of the structure – activity relationship for the free radical scavenging activity of baicalein. *J Mol Model*. 2011;17:2575–84.
29. Weigend F, Ahlrichs R. Balanced basis sets of split valence, triple zeta valence and quadruple zeta valence quality for H to Rn: Design and assessment of accuracy. *Phys Chem Chem Phys*. 2005;7(18):3297–305.
30. Molecular Operating Environment (MOE), 2015.02 Chemical Computing Group ULC, 1010 Sherbooke St. West, Suite #910, Montreal, QC, Canada, H3A 2R7, 2015.
31. Gasteiger J, Marsili M. Iterative partial equalization of orbital electronegativity—a rapid access to atomic charges. *Tetrahedron*. 1980;36(22):3219–28.
32. Lipinski CA, Lombardo F, Dominy BW, Feeney PJ. Experimental and computational approaches to estimate solubility and permeability in drug discovery and development settings. *Adv Drug Deliv Rev*. 1997;23:3–25.
33. Ahsan MJ, Samy JG, Khalilullah H, Nomani MS, Saraswat P, Gaur R, Singh A. Molecular properties prediction and synthesis of novel 1,3,4-oxadiazole analogues as potent antimicrobial and antitubercular agents. *Bioorganic Med Chem Lett*. 2011;21(24):7246–50.
34. Mazumdera J, Chakraborty R, Sena S, Vadras B, Dec B, Ravi TK. Synthesis and biological evaluation of some novel quinoxalanyl triazole derivatives. *Der Pharma Chem*. 2009;1(2):188–98.
35. Pires DEV, Blundell TL, Ascher DB. pkCSM: Predicting small-molecule pharmacokinetic and toxicity properties using graph-based signatures. *J Med Chem*. 2015;58(9):4066–72.
36. Rad AS, Ardjmand M, Esfahani MR, Khodashenas B. DFT calculations towards the geometry optimization, electronic structure, infrared spectroscopy and UV–vis analyses of Favipiravir adsorption on the first-row transition metals doped fullerenes; a new strategy for COVID-19 therapy. *Spectrochim Acta Part A Mol Biomol Spectrosc*. 2021;247:Article ID 119082.
37. Feynman R. The Feynman lectures on physics - Volume II. Millenium. Gottlieb MA, editor. New York: Basic Books; 2010; 11.3.